Enhancing Near-Field Radiative Heat Transfer with Si-based Metasurfaces

V. Fernández-Hurtado,[1,2,3] F. J. García-Vidal,[1,4] Shanhui Fan,[2] and J. C. Cuevas[1,3]
[1]Departamento de Física Teórica de la Materia Condensada and Condensed Matter Physics Center (IFIMAC), Universidad Autónoma de Madrid, E-28049 Madrid, Spain
[2]Department of Electrical Engineering, and Ginzton Laboratory, Stanford University, Stanford, California 94305, USA
[3]Department of Physics, University of Konstanz, D-78457 Konstanz, Germany
[4]Donostia International Physics Center (DIPC), Donostia/San Sebastián 20018, Spain
(Received 11 January 2017; published 15 May 2017)

We demonstrate in this work that the use of metasurfaces provides a viable strategy to largely tune and enhance near-field radiative heat transfer between extended structures. In particular, using a rigorous coupled wave analysis, we predict that Si-based metasurfaces featuring two-dimensional periodic arrays of holes can exhibit a room-temperature near-field radiative heat conductance much larger than any unstructured material to date. We show that this enhancement, which takes place in a broad range of separations, relies on the possibility to largely tune the properties of the surface plasmon polaritons that dominate the radiative heat transfer in the near-field regime.

DOI: 10.1103/PhysRevLett.118.203901

Thermal radiation is one of the most ubiquitous physical phenomena. In recent years, there has been a renewed interest in this topic due to the confirmation of the prediction that radiative heat transfer can be drastically enhanced for bodies separated by small gaps [1,2]. This occurs when the gap is smaller than the thermal wavelength (9.6 μm at room temperature), and it is due to the contribution of evanescent waves that dominate the near-field regime. The fact that this near-field radiative heat transfer (NFRHT) can overcome the far-field limit set by the Stefan-Boltzmann law has now been verified in a variety of experiments exploring different materials, geometrical shapes, and gaps ranging from micrometers to a few nanometers [3–17]. These experiments have also triggered off the hope that NFRHT could have an impact in different thermal technologies [18] such as thermophotovoltaics [19], heat-assisted magnetic recording [20,21], scanning thermal microscopy [22–24], nanolithography [25], thermal management [26,27], or coherent thermal sources [28,29].

In this context, the question on the fundamental limits of NFRHT is attracting a lot of attention [30]. So far, the largest NFRHT enhancements in extended structures have been reported for polar dielectrics (SiC, SiO_2, SiN, etc.), in which the NFRHT is dominated by surface phonon polaritons (SPhPs) [31,32]. There has not been any report of an extended structure that has a heat transfer coefficient exceeding that between two planar polar dielectric surfaces, and that includes metamaterials like hyperbolic ones [33,34]. In an attempt to tune NFRHT, several calculations of NFRHT between periodic metallic nanostructures in both 1D [35–38] and 2D [39] have been reported. These calculations have shown some degree of tunability and a NFRHT enhancement over the corresponding material without nanostructuration. However, the reported NFRHT in these structures is still smaller than in the case of parallel plates made of polar dielectrics. There have also been theoretical studies of the NFRHT between photonic crystals and periodic metamaterials made of dielectrics [40–42] that show how the radiative properties can be enhanced with respect to the bulk counterpart. However, the resulting NFRHTs are again much smaller than in planar polar dielectrics.

In this Letter, we show that metasurfaces of doped Si (see Fig. 1) can be used to boost NFRHT. Making use of a rigorous coupled wave analysis, we demonstrate that one can design Si metasurfaces that not only exhibit a room-temperature NFRHT much larger than that of bulk Si or other proposed periodic structures [39,41,42], but they also outperform the best unstructured polar dielectric

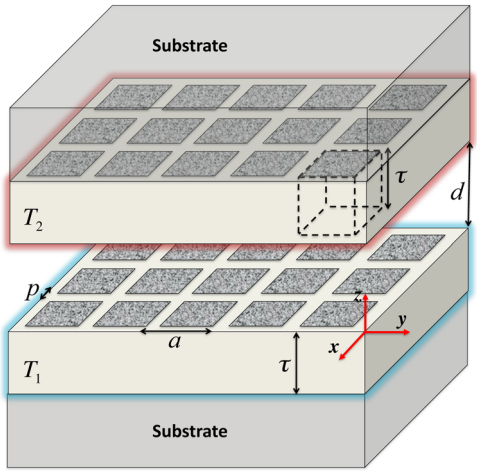

FIG. 1. Schematics of two doped-Si metasurfaces made of 2D periodic arrays of square holes placed on semi-infinite planar substrates and held at temperatures T_1 and T_2. The key parameters are shown: lattice parameter (a), distance between holes (p), gap size (d), and metasurface thickness (τ).

(SiO_2). By appropriately choosing the geometrical parameters of the metasurfaces, the enhancement over polar dielectrics occurs over a broad range of separations (from 13 nm to 2 μm). The underlying physical mechanisms responsible for this striking behavior are the existence of broadband surface-plasmon polaritons (SPPs) in doped Si and the ability to tune via nanostructuration the dispersion relation of these SPPs that dominate NFRHT in our structure. The predictions of this work show the great potential of metasurfaces for the field of NFRHT and can be tested with recent advances to measure NFRHT in parallel extended structures [16].

The system that we consider consists of two identical metasurfaces formed by 2D periodic arrays of square holes drilled in a doped Si layer; see Fig. 1. The metasurfaces are deposited on semi-infinite planar substrates. The geometrical parameters of the metasurfaces are the lattice constant a, the distance between holes p, the gap size d, and the thickness of the metasurfaces τ, which is equal to the depth of the holes in the structure. We define the filling factor of this structure as $f = (a-p)^2/a^2$, which describes the fraction of vacuum in the structure ($f = 0$ means no holes, while $f = 1$ means no Si). We focus on the analysis of the heat transfer coefficient, i.e., the linear radiative thermal conductance per unit of area, at room temperature (300 K). The dielectric function of doped Si is described within a Drude model [43]: $\epsilon_{\mathrm{Si}}(\omega) = \epsilon_\infty - \omega_p^2/(\omega^2 + i\gamma\omega)$, where $\epsilon_\infty = 11.7$, $\omega_p = 711$ meV is the plasma frequency, and $\gamma = 61.5$ meV is the damping. These values correspond to a doping level of 10^{20} cm^{-3}. The choice of this material and the doping level were motivated by the possibility to sustain SPPs at frequencies that can be thermally excited at room temperature. This is not possible for very high doping levels, while for very low ones the SPPs are not very confined and give a modest contribution to the NFRHT. Our main idea is that, by introducing holes in the Si layers, one can reduce the losses and the effective plasma frequency that, in turn, should redshift the surface modes. This way, these modes could be more easily occupied at room temperature, leading to an enhancement of the NFRHT.

To test this idea, we have combined the framework of fluctuational electrodynamics (FE) [2] with a rigorous coupled wave analysis (RCWA) [44] to compute NFRHT between periodic systems. In the frame of FE, the heat transfer coefficient (HTC) for two arbitrary periodic multilayer structures is given by [45]

$$h(d,T) = \int_0^\infty \frac{d\omega}{2\pi}\frac{\partial\Theta(\omega,T)}{\partial T}\int\frac{d\mathbf{k}_\parallel}{(2\pi)^2}\mathcal{T}(\omega,\mathbf{k}_\parallel), \quad (1)$$

where $\Theta(\omega,T) = \hbar\omega/[\exp(\hbar\omega/k_BT) - 1]$ is the mean energy of Planck oscillators at temperature T, ω is the angular frequency, $\mathbf{k}_\parallel = (k_x, k_y)$ is the wave vector parallel to the surface planes, and $\mathcal{T}(\omega,\mathbf{k}_\parallel)$ is the sum over polarizations of the transmission probability of the electromagnetic waves. The second integration in Eq. (1) is carried out over all possible directions of $\mathbf{k}_\parallel$, and it includes the contribution of both propagating waves with $k_\parallel < \omega/c$ and evanescent waves with $k_\parallel > \omega/c$, where $k_\parallel$ is the modulus of $\mathbf{k}_\parallel$ and c is the velocity of light in a vacuum. Within the RCWA approach, we express the fields in our periodic system as a sum of plane waves using the Bloch theorem. Thus, the transmission function above can be obtained by combining scattering matrices of the different interfaces in reciprocal space. In particular, if we place the coordinate origin at metasurface 1, the transmission coefficient can be expressed as [45]

$$\mathcal{T}(\omega,\mathbf{k}_\parallel) = \mathrm{Tr}\{\hat{D}\hat{W}_1\hat{D}^\dagger\hat{W}_2\}, \quad (2)$$

where

$$\hat{D} = (\hat{1} - \hat{S}_1\hat{S}_2)^{-1}, \quad (3)$$

$$\hat{W}_1 = \hat{\Sigma}_{-1}^{\mathrm{pw}} - \hat{S}_1\hat{\Sigma}_{-1}^{\mathrm{pw}}\hat{S}_1^\dagger + \hat{S}_1\hat{\Sigma}_{-1}^{\mathrm{ew}} - \hat{\Sigma}_{-1}^{\mathrm{ew}}\hat{S}_1^\dagger, \quad (4)$$

$$\hat{W}_2 = \hat{\Sigma}_{+1}^{\mathrm{pw}} - \hat{S}_2^\dagger\hat{\Sigma}_{+1}^{\mathrm{pw}}\hat{S}_2 + \hat{S}_2^\dagger\hat{\Sigma}_{+1}^{\mathrm{ew}} - \hat{\Sigma}_{+1}^{\mathrm{ew}}\hat{S}_2. \quad (5)$$

Here, $\hat{S}_1 = \hat{R}_1$ and $\hat{S}_2 = e^{ik_zd}\hat{R}_2e^{ik_zd}$, where $\hat{R}_1$ and $\hat{R}_2$ are the reflection matrices of the two vacuum-metasurface interfaces and $k_z^2 = \omega^2/c^2 - k_\parallel^2$. These matrices were computed with the scattering-matrix approach of Ref. [44]. Moreover, the matrix $\hat{\Sigma}_{-1(+1)}^{\mathrm{pw(ew)}}$ is a projector into the propagating (evanescent) sector. All these matrices are $2N_g \times 2N_g$ matrices, where N_g is the number of reciprocal lattice vectors included in the plane-wave expansions. On the other hand, the $\mathbf{k}$ integral in Eq. (1) must be calculated in the interval $(-\pi/a, \pi/a)$ for both k_x and k_y. A key point in our method is the use of the so-called fast Fourier factorization when dealing with the Fourier transform of two discontinuous functions in the Maxwell equations [44,46]. This factorization solves the known convergence problems of the RCWA approach.

Let us start the discussion of the results by illustrating the main finding of our work. For simplicity, we first assume that the Si layer thickness is infinite (no substrate). In Fig. 2(a), we show the room-temperature HTC as a function of the gap size for two metasurfaces with $a =$ 50 nm and $f = 0.9$. This result is compared with the HTC for two doped-Si and two SiO_2 parallel plates. Notice that the NFRHT between the Si metasurfaces is more than an order of magnitude larger than the corresponding result for Si plates for a broad range of separations. More importantly, the Si metasurfaces also exhibit a higher HTC than the silica plates in a broad distance range (from 13 nm to 2 μm), an enhancement that reaches a factor of 3 for gap sizes of about 100 nm. Let us emphasize that our structure exhibits a super-Planckian radiative heat transfer in that range of gaps (see arrow on the right). We also show in Fig. 2(a) the contribution of evanescent TM-polarized

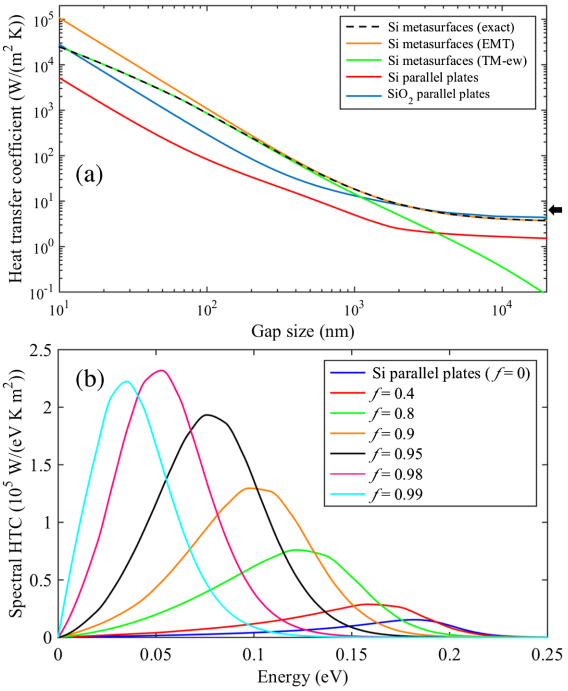

FIG. 2. (a) Room-temperature HTC as a function of the gap size for doped-Si metasurfaces with $a = 50$ nm and $f = 0.9$ (black dashed line). For comparison, we show the results for the Si metasurfaces computed with the effective medium theory (orange line), SiO_2 parallel plates (blue line), and doped-Si parallel plates (red line). The green line shows the contribution of evanescent TM-polarized waves to the HTC of the Si metasurfaces, and the arrow on the right indicates the blackbody limit, 6.1 $W/(m^2\ K)$. (b) Spectral HTC as a function of the photon energy for a gap of $d = 20$ nm and a lattice constant $a = 50$ nm. The different lines correspond to different filling factors.

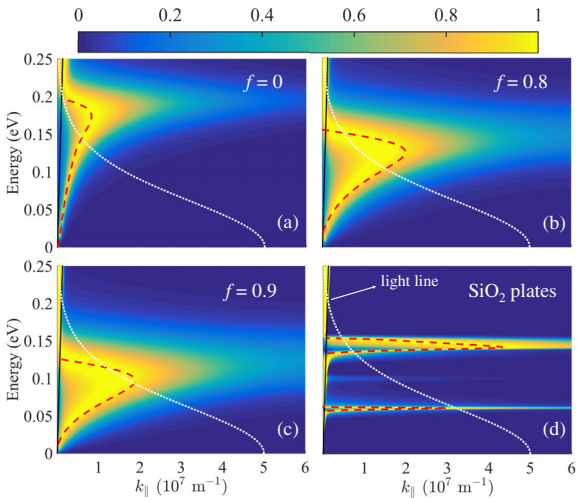

FIG. 3. Transmission of p-polarized waves along the x direction for $d = 20$ nm. (a)–(c) Si metasurfaces with lattice parameter $a = 50$ nm. The different panels correspond to various filling factors. The red dashed lines correspond to the dispersion relation of the SPPs [see Eq. (7)], and the black lines shows the dispersion relation of light in a vacuum. (d) The same as in the other panels but for two SiO_2 parallel plates. In this case, the red dashed line corresponds to the dispersion relation of the SPhPs in this structure. The white dotted lines in all panels correspond the occupation factor $\partial\Theta(\omega, T)/\partial T$ [see Eq. (1)] in arbitrary units.

waves to the HTC of the doped-Si metasurfaces. Notice that this contribution dominates the NFRHT for separations below 1 μm, which is a first hint that surface modes are responsible for the enhancement in this regime.

To get further insight into the role of the nanostructuration, we show in Fig. 2(b) the spectral HTC of the metasurfaces for a gap $d = 20$ nm, a lattice constant $a = 50$ nm, and different filling factors. This spectral HTC is defined as the HTC per unit of frequency or photon energy. As one can see, the maximum of the spectral HTC is redshifted upon increasing the size of the holes from 0.2 eV for $f = 0$ up to around 0.05 eV for $f = 0.98$. Notice also that the HTC (the integral of these spectral functions) also increases drastically with the filling factor, reaching a maximum at $f \approx 0.98$. These results illustrate the high tunability of NFRHT in metasurfaces.

The origin of the redshift in the spectral HTC can be understood with an analysis of the frequency and parallel wave vector dependence of the transmission $\mathcal{T}(\omega, \mathbf{k}_\parallel)$. Such a dependence is displayed in Fig. 3 for p-polarized waves, which dominate the NFRHT. In particular, we show the transmission along the x direction [$\mathbf{k}_\parallel = (k_x, 0)$] (see Fig. 1) for $d = 20$ nm, $a = 50$ nm, and different filling factors. As one can see in Fig. 3(a) for the case of two Si parallel plates ($f = 0$), the transmission maxima resemble the dispersion relation of a surface mode. As shown below, it corresponds to a cavity SPP mode that emerges from the hybridization of the SPP modes of the two vacuum-Si interfaces. Notice that the transmission maxima lie to the right of the light line (or dispersion relation of light in a vacuum), which indicates that these modes correspond to evanescent waves (both in a vacuum and inside Si). As the filling factor increases, we find that the transmission maxima redshift [see Figs. 3(b) and 3(c)], which is consistent with our observation above about the spectral HTC. Indeed, the frequency at which the maxima of the spectral HTC occur [see Fig. 2(b)] corresponds exactly to the position at which the transmission maxima fold back towards the light line. The reason is that in that frequency region the transmission is not only maximum, but also $k_\parallel$ takes the largest value, maximizing thus the density of photonic modes.

To confirm that cavity SPPs are indeed responsible for the NFRHT in our structure, we have analyzed their dispersion relation. For this purpose, we have made used of an effective medium theory (EMT) [47]. Within this theory, our metasurfaces can be modeled as uniaxial materials with a diagonal permittivity tensor: $\hat{\epsilon} = \mathrm{diag}(\epsilon_o, \epsilon_o, \epsilon_e)$, where the subindex o and e denote the ordinary and extraordinary optical axis, respectively. The components of the dielectric tensor are given by [47]

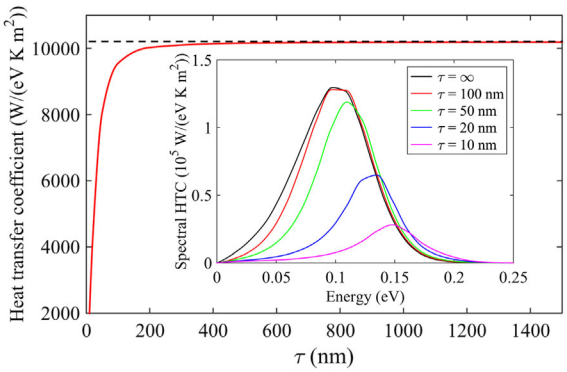

FIG. 4. Heat transfer coefficient as a function of the thickness of the periodically patterned Si layers for $d = 20$ nm, $a = 50$ nm, and $f = 0.9$. The dashed line corresponds to $\tau = \infty$. The inset shows the spectral HTC as a function of the energy for several metasurface thicknesses.

$$\epsilon_o = \epsilon_{\mathrm{Si}} \frac{\epsilon_{\mathrm{Si}}(1-f)+1+f}{\epsilon_{\mathrm{Si}}(1+f)+1-f}, \qquad \epsilon_e = f + (1-f)\epsilon_{\mathrm{Si}}. \tag{6}$$

In such a system, light propagates along the optical axes with perpendicular components of the wave vector given by $k_{z,o}^2 = \epsilon_o \omega^2/c^2 - k_\parallel^2$ and $k_{z,e}^2 = \epsilon_o \omega^2/c^2 - k_\parallel^2 \epsilon_o/\epsilon_e$. Within this approximation, the SPP dispersion relation is given by the solution of the following equation [48]:

$$e^{ik_z d} = \pm\left(\frac{k_{z,e} - \epsilon_o k_z}{k_{z,e} + \epsilon_o k_z}\right). \tag{7}$$

In the electrostatic limit ($k_\parallel \gg \omega/c$), this equation leads to the following dispersion relation for the cavity SPPs:

$$k_{\mathrm{SPP}}(\omega) = \frac{1}{d} \ln\left(\pm \frac{\epsilon_o(\omega) - \sqrt{\epsilon_o(\omega)/\epsilon_e(\omega)}}{\epsilon_o(\omega) + \sqrt{\epsilon_o(\omega)/\epsilon_e(\omega)}}\right). \tag{8}$$

The exact dispersion relations obtained from Eq. (7) are shown in Fig. 3 as red dashed lines. These dispersion relations nicely coincide with the transmission maxima for the whole range of filling factors, which unambiguously demonstrates that cavity SPPs dominate the NFRHT in our system. Moreover, this shows that NFRHT is drastically enhanced upon increasing the filling factor, because the surfaces modes shift to lower frequencies, which increases their thermal occupation at room temperature. This is illustrated in Fig. 3, where we show the frequency dependence of the factor $\partial\Theta(\omega, T)/\partial T$ that determines the occupation of these surface modes.

The enhancement of NFRHT in our metasurfaces over polar dielectrics like SiO_2 can be understood as follows. As we show in Fig. 3(d), the transmission between two silica plates is dominated by SPhPs [31], whose dispersion relation is given by Eq. (8) with $\epsilon_o = \epsilon_e = \epsilon_{\mathrm{SiO_2}}$ [13]. Although theses modes exhibit larger $k_\parallel$ values than the SPPs in our Si metasurfaces and therefore a larger photonic density of states, they are restricted to rather narrow frequency regions corresponding to the two reststrahlen bands in this material. Thus, the larger extension in frequency of the SPPs in the Si structures is one of the key factors that leads to a higher NFRHT.

The fact that the EMT nicely describes the position of the transmission maxima raises the question of whether this theory can also accurately describe the NFRHT. This is actually not the case, because the EMT assumes that the geometrical features are much smaller than the relevant physical length scales of the problem. In our case, where there is a considerable damping, the natural lateral scale is set by the propagation length of the cavity SPP wavelengths, $1/(2\mathrm{Im}\{k_{\mathrm{SPP}}\})$. For frequencies close to the folding back of the dispersion relation, which are the ones that dominate the spectral HTC, this propagation length can obtained from Eq. (8). Thus, for instance, for the structure analyzed in Fig. 2(a), Eq. (8) predicts that the SPP propagation length for the frequency of the spectral HTC maximum becomes of the order of the lattice parameter for $d \approx 100$ nm. Thus, the EMT is expected to fail below this gap size. To confirm this idea, we have computed the HTC in this structure within the EMT using the formalism for anisotropic planar systems of Ref. [48], and the result is shown in Fig. 2(a). As one can see, the EMT fails for gaps below the SPP propagation length. This analysis illustrates the need for an exact approach to accurately predict the NFRHT in these metasurfaces. Besides, the agreement between EMT results and the exact calculations for large gaps is evidence of the validity of our approach.

Let us stress that our periodic structures truly behave as metasurfaces, which can be understood as follows. From Eq. (8), we can estimate the penetration depth of the cavity SPPs, which in the electrostatic limit is given by $1/(2\mathrm{Re}\{k_{\mathrm{SPP}}\})$. Thus, we see that this penetration depth diminishes as the gap is reduced, which implies that the NFRHT is dominated by the surface of the periodic structures. Thus, for instance, for $d = 20$ nm, $a = 50$ nm, and $f = 0.9$, the penetration depth estimated from Eq. (8) is about 27 nm for the frequency of the spectral HTC maximum. Thus, one expects that all periodic structures with Si layers thicker than this penetration depth behave in the same way. To test this idea, we have computed the HTC as a function of the thickness of the periodic Si layers, τ, assuming that the substrate underneath is also made of (unstructured) doped Si. In Fig. 4, we show the results for this thickness dependence for the case mentioned above. Notice that when the layer thickness becomes larger than the gap, which is comparable to the SPP penetration depth, the HTC quickly tends to the result for a semi-infinite structure. This behavior is illustrated in the inset in Fig. 4 with the corresponding spectral HTCs. Thus, we can conclude that our periodic structures effectively behave as true metasurfaces as long as their thickness is larger than the gap size.

In summary, we have proposed a novel mechanism to further enhance NFRHT with the use of Si metasurfaces, which is based on the broad spectral bandwidth and high tunability of the SPPs that dominate NFRHT in these structures. We have shown that these metamaterials can exhibit room-temperature near-field radiative heat conductances higher than any existent or proposed structure. The fabrication of these metasurfaces is feasible with the state-of-the-art nanolithography [49], and our predictions could be tested with the recent developments in the measurement of NFRHT in parallel extended structures [16].

This work has been funded by "La Caixa" Foundation, the Spanish Ministry of Economy and Competitiveness (MINECO) under Contracts No. FIS2014-53488-P and No. MAT2014-53432-C5-5-R, the Comunidad de Madrid (Contract No. S2013/MIT-2740), and the European Research Council (ERC-2011-AdG Proposal No. 290981). J. C. C. and V. F.-H. thank the Deutsche Forschungsgemeinschaft (DFG) and Collaborative Research Center 767 (SFB 767) for sponsoring their stay at the University of Konstanz (J. C. C. for the Mercator Fellowship). S. F. acknowledges the support of the Global Climate and Energy Project (GCEP) at Stanford University and the U.S. Department of Energy "Light-Material Interactions in Energy Conversion" Energy Frontier Research Center under Grant No. DE-SC0001293.

[1] D. Polder and M. Van Hove, Theory of radiative heat transfer between closely spaced bodies, Phys. Rev. B **4**, 3303 (1971).
[2] S. M. Rytov, *Theory of Electric Fluctuations and Thermal Radiation* (Air Force Cambridge Research Center, Bedford, MA, 1953).
[3] A. Kittel, W. Müller-Hirsch, J. Parisi, S.-A. Biehs, D. Reddig, and M. Holthaus, Near-field Heat Transfer in a Scanning Thermal Microscope, Phys. Rev. Lett. **95**, 224301 (2005).
[4] E. Rousseau, A. Siria, G. Jourdan, S. Volz, F. Comin, J. Chevrier, and J.-J. Greffet, Radiative heat transfer at the nanoscale, Nat. Photonics **3**, 514 (2009).
[5] S. Shen, A. Narayanaswamy, and G. Chen, Surface phonon polaritons mediated energy transfer between nanoscale gaps, Nano Lett. **9**, 2909 (2009).
[6] R. S. Ottens, V. Quetschke, S. Wise, A. A. Alemi, R. Lundock, G. Mueller, D. H. Reitze, D. B. Tanner, and B. F. Whiting, Near-Field Radiative Heat Transfer between Macroscopic Planar Surfaces, Phys. Rev. Lett. **107**, 014301 (2011).
[7] T. Kralik, P. Hanzelka, M. Zobac, V. Musilova, T. Fort, and M. Horak, Strong Near-Field Enhancement of Radiative Heat Transfer between Metallic Surfaces, Phys. Rev. Lett. **109**, 224302 (2012).
[8] P. J. van Zwol, L. Ranno, and J. Chevrier, Tuning Near Field Radiative Heat Flux through Surface Excitations with a Metal Insulator Transition, Phys. Rev. Lett. **108**, 234301 (2012).
[9] P. J. van Zwol, S. Thiele, C. Berger, W. A. de Heer, and J. Chevrier, Nanoscale Radiative Heat Flow due to Surface Plasmons in Graphene and Doped Silicon, Phys. Rev. Lett. **109**, 264301 (2012).
[10] B. Guha, C. Otey, C. B. Poitras, S. H. Fan, and M. Lipson, Near-field radiative cooling of nanostructures, Nano Lett. **12**, 4546 (2012).
[11] L. Worbes, D. Hellmann, and A. Kittel, Enhanced Near-Field Heat Flow of a Monolayer Dielectric Island, Phys. Rev. Lett. **110**, 134302 (2013).
[12] R. St-Gelais, B. Guha, L. X. Zhu, S. H. Fan, and M. Lipson, Demonstration of strong near-field radiative heat transfer between integrated nanostructures, Nano Lett. **14**, 6971 (2014).
[13] B. Song, Y. Ganjeh, S. Sadat, D. Thompson, A. Fiorino, V. Fernández-Hurtado, J. Feist, F. J. Garcia-Vidal, J. C. Cuevas, P. Reddy, and E. Meyhofer, Enhancement of near-field radiative heat transfer using polar dielectric thin films, Nat. Nanotechnol. **10**, 253 (2015).
[14] K. Kim, B. Song, V. Fernández-Hurtado, W. Lee, W. Jeong, L. Cui, D. Thompson, J. Feist, M. T. H. Reid, F. J. Garcia-Vidal, J. C. Cuevas, E. Meyhofer, and P. Reddy, Radiative heat transfer in the extreme near field, Nature (London) **528**, 387 (2015).
[15] R. St-Gelais, L. Zhu, S. H. Fan, and M. Lipson, Near-field radiative heat transfer between parallel structures in the deep subwavelength regime, Nat. Nanotechnol. **11**, 515 (2016).
[16] B. Song, D. Thompson, A. Fiorino, Y. Ganjeh, P. Reddy, and E. Meyhofer, Radiative heat conductances between dielectric and metallic parallel plates with nanoscale gaps, Nat. Nanotechnol. **11**, 509 (2016).
[17] M. P. Bernardi, D. Milovich, and M. Francoeur, Radiative heat transfer exceeding the blackbody limit between macroscale planar surfaces separated by a nanosize vacuum gap, Nat. Commun. **7**, 12900 (2016).
[18] B. Song, A. Fiorino, E. Meyhofer, and P. Reddy, Near-field radiative thermal transport: From theory to experiment, AIP Adv. **5**, 053503 (2015).
[19] A. Lenert, D. M. Bierman, Y. Nam, W. R. Chan, I. Celanovic, M. Soljacic, and E. N. Wang, A nanophotonic solar thermophotovoltaic device, Nat. Nanotechnol. **9**, 126 (2014).
[20] W. A. Challener, C. B. Peng, A. V. Itagi, D. Karns, W. Peng, Y. Y. Peng, X. M. Yang, X. B. Zhu, N. J. Gokemeijer, Y. T. Hsia, G. Ju, R. E. Rottmayer, M. A. Seigler, and E. C. Gage, Heat-assisted magnetic recording by a near-field transducer with efficient optical energy transfer, Nat. Photonics **3**, 220 (2009).
[21] B. C. Stipe, T. C. Strand, C. C. Poon, H. Balamane, T. D. Boone, J. A. Katine, J. L. Li, V. Rawat, H. Nemoto, A. Hirotsune, O. Hellwig, R. Ruiz, E. Dobisz, D. S. Kercher, N. Robertson, T. R. Albrecht, and B. D. Terris, Magnetic recording at 1.5 Pb m^{-2} using an integrated plasmonic antenna, Nat. Photonics **4**, 484 (2010).
[22] Y. D. Wilde, F. Formanek, R. Carminati, B. Gralak, P. A. Lemoine, K. Joulain, J. P. Mulet, Y. Chen, and J. J. Greffet, Thermal radiation scanning tunnelling microscopy, Nature (London) **444**, 740 (2006).
[23] A. Kittel, U. F. Wischnath, J. Welker, O. Huth, F. Ruting, and S. A. Biehs, Near-field thermal imaging of nanostructured surfaces, Appl. Phys. Lett. **93**, 193109 (2008).

[24] A. C. Jones, B. T. O'Callahan, H. U. Yang, and M. B. Raschke, The thermal near-field: Coherence, spectroscopy, heat-transfer, and optical forces, Prog. Surf. Sci. **88**, 349 (2013).
[25] J. B. Pendry, Radiative exchange of heat between nanostructures, J. Phys. Condens. Matter **11**, 6621 (1999).
[26] C. Otey, W. T. Lau, and S. Fan, Thermal Rectification through Vacuum, Phys. Rev. Lett. **104**, 154301 (2010).
[27] P. Ben-Abdallah and S. A. Biehs, Near-Field Thermal Transistor, Phys. Rev. Lett. **112**, 044301 (2014).
[28] R. Carminati and J. J. Greffet, Near-Field Effects in Spatial Coherence of Thermal Sources, Phys. Rev. Lett. **82**, 1660 (1999).
[29] J. J. Greffet, R. Carminati, K. Joulain, J. P. Mulet, S. P. Mainguy, and Y. Chen, Coherent emission of light by thermal sources, Nature (London) **416**, 61 (2002).
[30] O. D. Miller, S. G. Johnson, and A. W. Rodriguez, Shape-Independent Limits to Near-Field Radiative Heat Transfer, Phys. Rev. Lett. **115**, 204302 (2015).
[31] J. P. Mulet, K. Joulain, R. Carminati, and J. J. Greffet, Enhanced radiative heat transfer at nanometric distances, Microscale Thermophys. Eng. **6**, 209 (2002).
[32] H. Iizuka and S. Fan, Analytical treatment of near-field electromagnetic heat transfer at the nanoscale, Phys. Rev. B **92**, 144307 (2015).
[33] S. A. Biehs, M. Tschikin, and P. Ben-Abdallah, Hyperbolic Metamaterials as an Analog of a Blackbody in the Near Field, Phys. Rev. Lett. **109**, 104301 (2012).
[34] O. D. Miller, S. G. Johnson, and A. W. Rodriguez, Effectiveness of Thin Films in Lieu of Hyperbolic Metamaterials in the Near Field, Phys. Rev. Lett. **112**, 157402 (2014).
[35] R. Guérout, J. Lussange, F. S. S. Rosa, J.-P. Hugonin, D. A. R. Dalvit, J. J. Greffet, A. Lambrecht, and S. Reyanud, Enhanced radiative heat transfer between nanostructured gold plates, Phys. Rev. B **85**, 180301(R) (2012).
[36] J. Dai, S. A. Dyakov, and M. Yan, Enhanced near-field radiative heat transfer between corrugated metal plates: Role of spoof surface plasmon polaritons, Phys. Rev. B **92**, 035419 (2015).
[37] J. Dai, S. A. Dyakov, and M. Yan, Radiative heat transfer between two dielectric-filled metal gratings, Phys. Rev. B **93**, 155403 (2016).
[38] R. Messina, A. Noto, B. Guizal, and M. Antezza, Radiative heat transfer between metallic gratings using adaptive spatial resolution, Phys. Rev. B **95**, 125404 (2017).
[39] J. Dai, S. A. Dyakov, S. I. Bozhevolnyi, and M. Yan, Near-field radiative heat transfer between metasurfaces: A full-wave study based on two-dimensional grooved metal plates, Phys. Rev. B **94**, 125431 (2016).
[40] A. W. Rodriguez, O. Ilic, P. Bermel, I. Celanovic, J. D. Joannopoulos, M. Soljacic, and S. G. Johnson, Frequency-Selective Near-Field Radiative Heat Transfer between Photonic Crystal Slabs: A Computational Approach for Arbitrary Geometries and Materials, Phys. Rev. Lett. **107**, 114302 (2011).
[41] X. Liu and Z. M. Zhang, Enhanced near-field thermal radiation and reduced Casimir stiction between doped-Si gratings, Phys. Rev. A **91**, 062510 (2015).
[42] X. Liu and Z. M. Zhang, Near-field thermal radiation between metasurfaces, ACS Photonics **2**, 1320 (2015).
[43] S. Basu, B. J. Lee, and Z. M. Zhang, Infrared radiative properties of heavily doped silicon at room temperature, J. Heat Transfer **132**, 023301 (2010).
[44] B. Caballero, A. García-Martín, and J. C. Cuevas, Generalized scattering-matrix approach for magneto-optics in periodically patterned multilayer systems, Phys. Rev. B **85**, 245103 (2012).
[45] G. Bimonte, Scattering approach to Casimir forces and radiative heat transfer for nanostructured surfaces out of thermal equilibrium, Phys. Rev. A **80**, 042102 (2009).
[46] L. Li, New formulation of the Fourier modal method for crossed surface-relief gratings, J. Opt. Soc. Am. A **14**, 2758 (1997).
[47] X. L. Liu, L. P. Wang, and Z. M. Zhang, Wideband tunable omnidirectional infrared absorbers based on doped silicon nanowire arrays, J. Heat Transfer **135**, 061602 (2013).
[48] E. Moncada-Villa, V. Fernández-Hurtado, F. J. García-Vidal, A. García-Martin, and J. C. Cuevas, Magnetic field control of near-field heat transfer and the realization of highly tunable hyperbolic thermal emitters, Phys. Rev. B **92**, 125418 (2015).
[49] V. R. Manfrinato, L. Zhang, D. Zu, H. Duan, R. G. Hobbs, E. A. Stachand, and K. K. Berggren, Resolution limits of electron-beam lithography toward the atomic scale, Nano Lett. **13**, 1555 (2013).